FRONTIERS OF PHYSICS

RESEARCH ARTICLE
Volume 19 / Issue 6 / 63204 / 2024

Key electronic parameters of 2*H*-stacking bilayer MoS_2 on sapphire substrate determined by terahertz magneto-optical measurement in Faraday geometry

Xingjia Cheng[1,2], Wen Xu[1,3,4,†], Hua Wen[1,2], Jing Zhang[1,2], Heng Zhang[1,2], Haowen Li[4], Francois M. Peeters[4,5]

1 Key Laboratory of Materials Physics, Institute of Solid State Physics, HFIPS, Chinese Academy of Sciences, Hefei 230031, China
2 University of Science and Technology of China, Hefei 230026, China
3 School of Physics and Astronomy and Yunnan Key Laboratory of Quantum Information of Yunnan Province, Yunnan University, Kunming 650091, China
4 Micro Optical Instruments Inc., Shenzhen 518118, China
5 Department of Physics, University of Antwerp, Groenenborgerlaan 171, B-2020 Antwerpen, Belgium
Corresponding author. E-mail: †wenxu_issp@aliyun.com
Received January 27, 2024; accepted May 27, 2024

ABSTRACT

Bilayer (BL) transition metal dichalcogenides (TMDs) are important materials in valleytronics and twistronics. Here we study terahertz (THz) magneto-optical (MO) properties of n-type 2*H*-stacking BL molybdenum sulfide (MoS_2) on sapphire substrate grown by chemical vapor deposition. The AFM, Raman spectroscopy and photoluminescence are used for characterization of the samples. Applying THz time-domain spectroscopy (TDS), in combination with polarization test and the presence of magnetic field in Faraday geometry, THz MO transmissions through the sample are measured from 0 to 8 T at 80 K. The complex right- and left-handed circular MO conductivities for 2*H*-stacking BL MoS_2 are obtained. Through fitting the experimental results with theoretical formula of MO conductivities for an electron gas, generalized by us previously through the inclusion of photon-induced electronic backscattering effect, we are able to determine magneto-optically the key electronic parameters of BL MoS_2, such as the electron density n_e, the electronic relaxation time τ, the electronic localization factor c and, particularly, the effective electron mass m^* around Q-point in between the K- and Γ-point in the electronic band structure. The dependence of these parameters upon magnetic field is examined and analyzed. This is a pioneering experimental work to measure m^* around the Q-point in 2*H*-stacking BL MoS_2 and the experimental value is very close to that obtained theoretically. We find that $n_e/\tau/|c|/m^*$ in 2*H*-stacking BL MoS_2 decreases/increases/decreases/increases with increasing magnetic field. The results obtained from this study can be benefit to us in gaining an in-depth understanding of the electronic and optoelectronic properties of BL TMD systems.

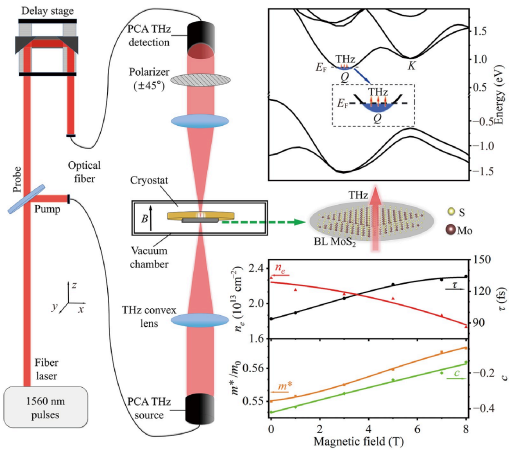

Keywords bilayer MoS_2, terahertz time-domain spectroscopy, magneto-optical conductivities, key electronic parameters, effective electron mass

https://doi.org/10.1007/s11467-024-1425-4

1 Introduction

Two-dimensional (2D) transition metal disulfides (TMDs) have been proposed as advanced electronic and optoelectronic materials beyond silicon [1]. It is known that monolayer (ML) TMD is with the unique valley related electronic properties which can be utilized to realize the valleytronic devices for, e.g., information processing and storage [2]. Since the discovery of superconductivity in bilayer (BL) graphene [3], the fabrication and investigation of BL TMD systems have become the hot and fast-growing field of research in condensed matter physics, electronics, optics and optoelectronics [4–7]. The BL structures can provide one more degree of freedom in achieving new lattice configuration via translation and/or rotation of one layer on another layer. This has opened up a new field of research as twistronics [8]. BL TMD materials are important not only in spintronics and valleytronics but also in twistronics [6, 9], evident by the discoveries of, e.g., the topological mosaics in moiré superlattices [10], inter-layer excitons [11], anomalous Nernst effect [12], and spin-layer locking effect [13]. At present, the easy way to realize experimentally the high symmetric BL TMD is to fabricate the homogenous TMD BLs via superposing two ML TMD grown by chemical vapor deposition (CVD) on a dielectric substrate [6]. The high symmetric homogenous BL TMD structures are important category of BL electronic systems. ML TMD, such as MX_2 with M = Mo or W and X = S or Se, is a hexagonal crystal in which the metal atom (M) is sandwiched between the chalcogen atoms (X) on both sides. The homogenous TMD BLs with six types of high symmetric stacking orders can be formed as H^M_X or $2H$, H^M_M, H^X_X, R^M_M, R^M_X, and R^X_M. These stacking structures satisfy the C_3 symmetry. From a viewpoint of condensed matter physics, the electronic band structures in these BL TMD differ significantly from that in ML TMD [14]. ML TMD is a direct band gap semiconductor in which the lowest/highest conduction/valence band is around K/K' point. As a result, the strong photoluminescence (PL) and inter-band optical absorption induced by inter-band electronic transition can be observed experimentally from ML TMD [15]. In contrast, the features of the direct band gap semiconductor are much weaker in homogenous BL TMD owing to inter-layer interaction [16]. Particularly, it is found that the conduction band minima in $2H$-stacking BL TMD is at Σ_{min}- or Q-point [17, 18] which is in-between the K and Γ point. Therefore, the electrons mainly occupy the Q-point in n-type $2H$-stacking BL TMD in low electron density samples. For the application of $2H$-stacking BL TMD as electronic and optoelectronic material, it is of significance and importance to investigate the basic electronic properties of Q-point in BL TMD with high symmetric $2H$-stacking configuration, which becomes the prime motivation of the present study.

From theoretical findings obtained from DFT calculations [17, 18], we learn that in $2H$-stacking BL TMD such as MoS_2, the valence band around the Q-point shows a deep valley, indicating that the Q-point is with an indirect band gap lager than 2 eV [18]. The weak feature of the direct band gap can be observed around K-point so that the weak PL emission can be measured [18, 19]. Due to these features of electronic band structure, it is not easy and straight forward to extract the electronic information around Q-point by conventional infrared and visible optical measurements on $2H$-stacking BL TMD. The electronic transition accompanied by the emission and absorption of photons from Q-point can only be achieved via indirect channels mediated by, e.g., phonon scattering, evident by the observation of an extra "a" peak in Raman spectrum [18]. Thanks to the development of terahertz (THz) optoelectronic technology, now it is possible to measure the free-electron dynamics in electronic materials by using, e.g., THz time-domain spectroscopy (TDS) [20, 21]. Due to relatively small energy of THz photons ($f = 1$ THz is about 4.13 meV), the respond of electrons to THz radiation field can be achieved via intra-band electronic transition around the Fermi energy. The THz radiation do not induce inter-band transition and photon-generated carriers. Therefore, THz TDS is very suitable to the study of electronic properties induced by the occupancy of electrons around the Q-point in $2H$-stacking BL TMD. Very recently, we have applied the THz TDS to study the THz optoelectronic properties of n-type $2H$-stacking BL MoS_2 on sapphire substrate [18]. The key electronic parameters of the sample, such as the electron density, the electronic relaxation time and photon-induced electronic localization factor have been measured optically. The temperature dependence of these parameters have been examined. It should be noted that at present, the effective electron mass around the Q-point in $2H$-stacking BL TMD has not yet been measured experimentally. We used the theoretical value of it for the fitting with our experimental results [18].

It is known that the magneto-optical (MO) measurement is a powerful technique for studying and characterizing of the electronic materials [22], from which more details and information of the electronic structure of the sample can be obtained. In recent years, infrared and visible MO techniques have been applied to study TMD based BL structures. For example, in 2022 Campbell and coworkers [23] applied the visible MO measurements to reveal the anomalous Zeeman splitting of exciton polaritons in $MoSe_2/WSe_2$ twisted heterostructures induced by exchange interaction, demonstrating the rich potential of the $MoSe_2/WSe_2$ platform in Fermi–Hubbard and Bose–Hubbard physics. We demonstrated previously that THz MO measurement can be applied to determine the effective electron mass in electronic materials such as bi- and tri-layer graphene under non-resonant condition [24]. In this study, we intend to apply THz TDS in the

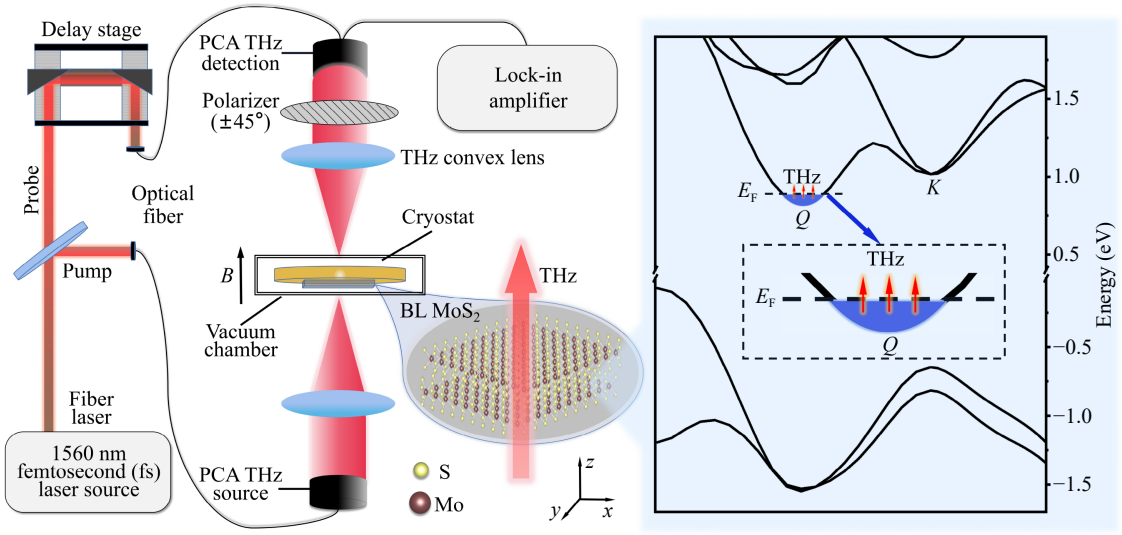

Fig. 1 Left panel: Schematic diagram of the THz TDS system for MO transmission measurement of BL MoS_2 on sapphire substrate. Here, the measurement is undertaken in the Faraday geometry where both the incident THz beam, which is linearly polarized, and the magnetic field B are applied perpendicularly to the sample surface, and a polarizer is applied to examine the polarization of the transmitted THz beam. Right panel: The electronic band structure of 2H-stacking BL MoS_2 [18], where the inset shows the electronic transition around the Fermi level E_F in the Q-band in an n-type BL MoS_2 under the action of THz driving. The blue area in the Q-band presents the populated electronic states.

presence of strong magnetic field for the examination of the THz MO properties of n-type 2H-stacking BL MoS_2 and for the determination of the effective electron mass around the Q-point.

2 Samples and experimental measurements

2.1 Sample preparation and characterization

In this study, BL MoS_2 films were grown on sapphire substrate by using the standard chemical vapor deposition (CVD) in combination with the poly-dimethylsiloxane (PDMS) wet transfer method [25, 26]. The procedures and details for the growth and preparation of 2H-stacking BL MoS_2 placed on the sapphire substrate are the same as in our previous work (see Fig. 1 in Ref. [18]). BL MoS_2 on sapphire substrate fabricated by this technique is normally the n-type [18], which was confirmed by our Hall measurement. The areal size of the sample and the thickness of the substrate are 1 cm × 1 cm and 0.3 mm, respectively. The realization of 2H-stacking BL MoS_2 on the substrate was verified by the measurements of the AFM [27, 28], Raman spectroscopy [27, 28] and photoluminescence [29, 30]. The results obtained from sample characterization are presented in Supplementary Materials.

2.2 Terahertz magneto-optical transmission in Faraday geometry

The THz MO measurements in this work are carried out in the standard Faraday geometry, where both the magnetic field and the incident THz light beam are applied perpendicularly to the surface of BL MoS_2 sample, as shown in Fig. 1. In this configuration, the linearly polarized radiation field can couple with the magnetic field through electrons in the measured sample. The details of the experimental setup for the measurement are as follows. i) 1560 nm femtosecond (fs) laser beam (RIO Optoelectronics. The repetition rate is 100 MHz and pulse duration is 80 fs) is divided into two beams as the pump and detection light sources respectively; ii) The fs pump laser is focused on an InGaAs photoconductance antenna (PCA, Menlo, Germany) to generate pulsed THz radiation which is highly linearly polarized; iii) The incident THz beam is applied normally and focused on the surface of BL MoS_2 sample placed on a sample holder in a cryostat (ST-500, Janis, UK) with two quartz windows. We note that because the quartz window absorbs the high-frequency THz light [31], the effective spectral regime for the measurement is limited to about 0.2 to 1.0 THz in the present study; iv) A superconducting magnet (Gryomagnetics, USA) is used to apply and tune the strength of magnetic field B from 0 to 8 T; v) The fs detection laser is focused, after the time delay by a delay stage, on another InGaAs PCA for the detection of THz beam transmitted through the BL MoS_2 sample via electro-optical sampling. Thus, we can record the THz electric field transmitted through the sample as a function of the delay time; and vi) a wire gird polarizer made of polyethylene (TYDEX, Russia) is used to examine the polarization of the THz

transmission beam. In this measurement setup, the incident THz beam and the B field are applied along the z-direction and the polarization angles of the polarizer are set to be at $\pm 45°$ to the polarization direction of the incident THz beam (taken along the x-direction). The system is sealed in a nitrogen gas environment to reduce the effect of THz absorption by moisture and dust. In this study, the measurements are conducted at 80 K with liquid nitrogen in the cryostat.

In the right panel of Fig. 1, we present the electronic band structure of 2H-stacking BL MoS_2. The inset shows a schematic diagram of electronic transition in the Q-band in a n-type BL MoS_2 under the action of THz radiation. Because the THz photon energy is relatively small ($f = 1$ THz ~ 4.13 meV), THz pump can only cause the electron transitions around the Fermi level E_F and THz probe can detect the dynamical response of electrons around E_F in BL MoS_2. Because the energy difference between the K- and Q-point in 2H-stacking BL MoS_2 is about 197 meV [18], the conducting electrons predominantly occupy the Q-point in 2H-stacking BL MoS_2.

Using this experimental setup, we can measure the THz transmission electric field strength at $\pm 45°$ polarization angles of the polarizer, $E_{\pm 45°,j}(t)$, as a function of delay time t for the sample (i.e., $j = \text{sample}$ for BL MoS_2 on the substrate) and for the bare substrate (i.e., $j = \text{substrate}$) respectively at a fixed B. By Fourier transformation of these data, we can obtain the corresponding electric field strengths of the sample and the substrate in the frequency domain $E_{\pm 45°,j}(\omega)$. Because of the Fourier transformation, $E_{\pm 45°,j}(\omega)$ is a complex quantity. According to the Fresnel theory [24, 32], the linearly polarized light field can be decomposed into the left- and right-handed circular polarized (RHCP and LHCP) light modes via [33]

$$\begin{pmatrix} E_{+,j}(\omega) \\ E_{-,j}(\omega) \end{pmatrix} = \frac{1}{2} \begin{pmatrix} \mathrm{i}-1 & \mathrm{i}+1 \\ \mathrm{i}+1 & \mathrm{i}-1 \end{pmatrix} \times \begin{pmatrix} E_{+45°,j}(\omega) \\ E_{-45°,j}(\omega) \end{pmatrix}. \tag{1}$$

Thus, the transmission coefficients for the RHCP (+) and LHCP (−) components of the BL MoS_2 can be evaluated approximately by [32]

$$t_{\pm}(\omega) = \frac{E_{\pm,\text{sample}}(\omega)}{E_{\pm,\text{substrate}}(\omega)}. \tag{2}$$

2.3 Terahertz magneto-optical conductivities

For an air/BL MoS_2/substrate/air system in which the thickness of BL MoS_2 film is much less than the wavelength of THz radiation field (1 THz $\sim$ 300 μm), the relationship between the RHCP and LHCP transmission coefficients and the corresponding MO conductivities can be found by the Tinkham formula [34]

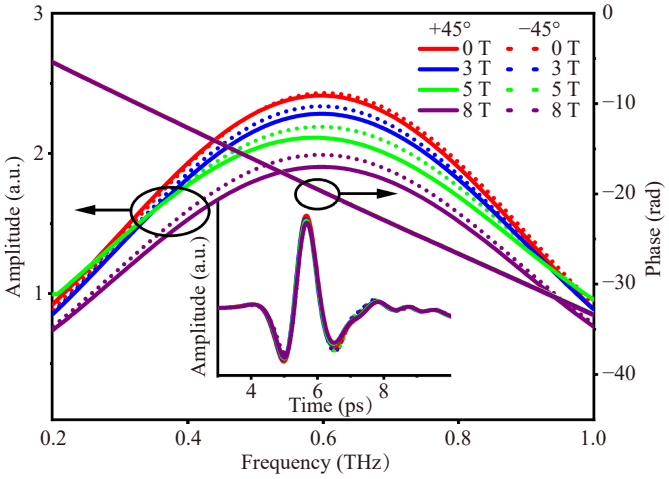

Fig. 2 Amplitude and phase angle of $E_{\pm 45°,\text{sample}}(\omega)$ of the THz electric field transmitted through the BL MoS_2 sample as a function of radiation frequency $f = \omega/(2\pi)$ in different magnetic fields as indicated. The results for the phase angles coincide roughly. The inset shows $E_{\pm 45°,\text{sample}}(t)$ of the THz electric field transmitted through the sample as a function of delay time.

$$t_{\pm}(\omega) = \frac{1 + N_s}{1 + N_s + Z_0\sigma_{\pm}(\omega)}, \tag{3}$$

where N_s is the refractive index of the substrate (for sapphire, $N_s = 3.07$), $Z_0 = 377\ \Omega$ is the impedance of free space, and $\sigma_{\pm}(\omega) = \sigma_{\pm 1}(\omega) + \mathrm{i}\sigma_{\pm 2}(\omega)$ is the RHCP (+) or LHCP (−) MO conductivity. Once $\sigma_{\pm}(\omega)$ is obtained, the longitudinal and transverse MO conductivities for BL MoS_2 film can also be obtained via

$$\sigma_{xx}(\omega) = [\sigma_+(\omega) + \sigma_-(\omega)]/2,$$

and

$$\sigma_{xy}(\omega) = [\sigma_+(\omega) - \sigma_-(\omega)]/(2i). \tag{4}$$

3 Results and discussion

3.1 THz MO transmission spectra and conductivities

The THz electric field strength transmitted through the BL MoS_2 sample as a function of delay time, $E_{\pm 45°,\text{sample}}(t)$, is shown in the inset in Fig. 2 at different magnetic fields. We can see that $E_{+45°,\text{sample}}(t)$ differs from $E_{-45°,\text{sample}}(t)$ and they both depend on the strength of the magnetic field. The amplitude and the phase angle of the THz electric field, $E_{\pm 45°,\text{sample}}(\omega)$, transmitted through the BL MoS_2 sample as a function of radiation frequency is presented in Fig. 2 at the magnetic field $B =$ 0, 3, 5, and 8 T. We notice that: i) the magnetic field and the $\pm 45°$ polarization angles affect mainly the amplitude of $E_{\pm 45°,\text{sample}}(\omega)$. The phase angle of $E_{\pm 45°,\text{sample}}(\omega)$ depends very weakly on B and the polarization angle;

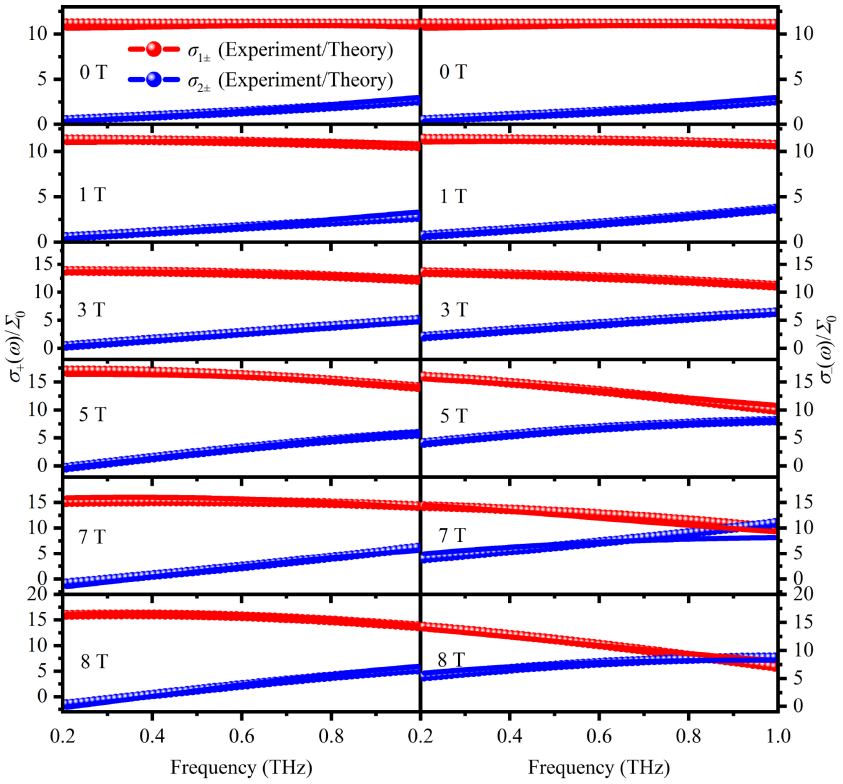

Fig. 3 Real $\sigma_{1\pm}(\omega)$ (red dots and curves) and imaginary $\sigma_{2\pm}(\omega)$ (blue dots and curves) parts of RHCP and LHCP MO conductivities for BL MoS_2 as a function of radiation frequency $f = \omega/(2\pi)$ in different magnetic fields as indicated. Here, the results for $\sigma_+(\omega)$ and $\sigma_-(\omega)$ are shown respectively in the left and right panels, the dots are experimental results, the curves are obtained from Eq. (7), and $\Sigma_0 = e^2/(4\hbar) = 6.07 \times 10^{-5}$ S.

ii) the amplitude $|E_{\pm 45^\circ,\text{sample}}(\omega)|$ decreases with increasing of B; iii) the phase angles of $E_{\pm 45^\circ,j}(\omega)$ decrease almost linearly with increasing THz radiation frequency; and iv) at a fixed B, $|E_{-45^\circ,\text{sample}}(\omega)|$ is larger than $|E_{+45^\circ,\text{sample}}(\omega)|$, indicating that the BL MoS_2 sample can rotate the incident THz light in the presence of magnetic field. These results demonstrate that $2H$-stacking BL MoS_2 placed on sapphire substrate can induce THz MO response strongly.

In Fig. 3, we show the real and imaginary parts of $\sigma_\pm(\omega)$ obtained by Eq. (3) as a function of radiation frequency. It can be seen that both $\sigma_{1\pm}(\omega)$ and $\sigma_{2\pm}(\omega)$ increase with B. $\sigma_{1-}(\omega)$ decreases and $\sigma_{2-}(\omega)$ increases with increasing $f = \omega/(2\pi)$ quite markedly. In contrast, $\sigma_{1+}(\omega)$ and $\sigma_{2+}(\omega)$ depend rather weakly on f. It should be noted that the real part $\sigma_{1\pm}(\omega)$ is related to the energy dissipation or light absorption caused by electron –photon interaction when scattering centers such as impurities and phonons are present, while the imaginary part $\sigma_{2\pm}(\omega)$ corresponds to the energy exchange between the electron and the externa field, during which the energy of the electron field system does not altered. We find that at $T = 80$ K and $B = 0$ to 8 T, no significant quantum effects can be observed in the real and imaginary parts of $\sigma_\pm(\omega)$ for our BL MoS_2 sample (Fig. 3). This is mainly owing to the fact that BL MoS_2 is of relatively heavy effective electron mass and our sample is with relatively low electron mobility. Therefore, we can employ the theoretical formula of MO conductivities for free-electrons in understanding our experimental results. We first used the conventional Drude model for MO conductivities [24, 35] to fit our experimental results and found that the fittings were poor. In this study, we apply the MO conductivities obtained from Drude–Smith model to understand and fit our experimental results. In 2001 Smith [36] proposed a modified model to calculate the optical conductivity of free electrons at $B = 0$, which took into account of impulse response and Poisson statistics for the inclusion of electronic backscattering effect. Thus, the effect of photon-induced electron backscattering or localization can be considered. In 2016, we generalized this approach to the case where a magnetic field is present in the Faraday geometry and derived the corresponding longitudinal and transverse MO conductivities [35], which read

$$\sigma_{xx}(\omega) = \frac{\sigma_0(1 - \mathrm{i}\omega\tau)}{(1 - \mathrm{i}\omega\tau)^2 + (\omega_c\tau)^2} + \frac{c\sigma_0}{2}\left[\frac{1}{[1 - \mathrm{i}(\omega + \omega_c)\tau]^2} + \frac{1}{[1 - \mathrm{i}(\omega - \omega_c)\tau]^2}\right], \tag{5}$$

and

$$\sigma_{xy}(\omega) = -\frac{\sigma_0\omega_c\tau}{(1-\mathrm{i}\omega\tau)^2+(\omega_c\tau)^2} + \frac{\mathrm{i}c\sigma_0}{2}\left[\frac{1}{[1-\mathrm{i}(\omega+\omega_c)\tau]^2} - \frac{1}{[1-\mathrm{i}(\omega-\omega_c)\tau]^2}\right], \tag{6}$$

where $\sigma_0 = n_e e^2\tau/m^*$ is the D.C. conductivity at $B = 0$, n_e is the electron density in BL MoS_2, τ is the electron relaxation time, m^* is the effective electron mass, and $\omega_c = eB/m^*$ is the cyclotron frequency. In addition, the factor $c = [-1, 0]$ represents the proportion of the original velocity of an electron after the collision event. It is known that the Drude-like optical conductivity can be derived theoretically on the basis of the current response function for an electron gas system [36], where the initial current depends on band parameter such as the effective electron mass and on electron density and decays exponentially to its equilibrium value with a relaxation time τ. The complex form of the optical conductivity in frequency domain can be obtained by the Fourier transformation of the current response function. After considering the fact that an electron in a material may suffer the first and subsequent collisions due to backscattering mechanism, the current response function can be modified by the inclusion of a Poisson distribution on top of the exponential decay in different backscattering events [36]. Thus, this model has been taken into consideration that an electron experiences collisions which are randomly distributed in time but with an average time interval τ between collision events. Hence, the modification proposed in the Drude–Smith model or the inclusion of the electronic backscattering in the current response function does not directly relate to the electronic energy-band structure of the material, implying that the model is generally independent upon the materials from a theoretical point of view.

In Eq. (5) and Eq. (6), we consider only the first collision term in the general MO Drude–Smith formula [35]. When c tends to -1 the electrons in the system are fully localized so that $\sigma_{xx}(0) = \sigma_{xy}(0) = 0$, while when $c = 0$ the MO conductivities become those given by the conventional Drude–Smith formula [36]. From $\sigma_{xx}(\omega)$ and $\sigma_{xy}(\omega)$, we obtain RHCP and LHCP MO conductivities simply as [32]

$$\sigma_{\pm}(\omega) = \sigma_{xx}(\omega) \pm \mathrm{i}\sigma_{xy}(\omega) = \sigma_{1\pm}(\omega) + \mathrm{i}\sigma_{2\pm}(\omega) = \frac{\sigma_0(1-\mathrm{i}\omega\tau \pm \mathrm{i}\omega_c\tau + c)}{(1-\mathrm{i}\omega\tau \pm \mathrm{i}\omega_c\tau)^2}. \tag{7}$$

As can be seen from Fig. 3, $\sigma_{1\pm}(\omega)$ and $\sigma_{2\pm}(\omega)$ given by MO Drude–Smith model of Eq. (7) can correctly describe the dependence of the real and imaginary parts of $\sigma_{\pm}(\omega)$ upon the strength of B and the THz radiation frequency f.

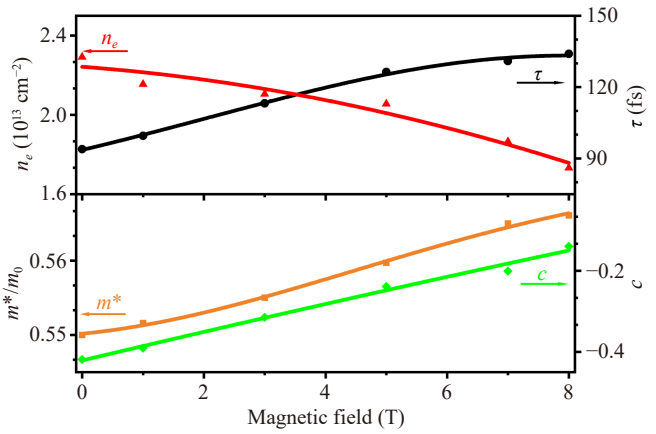

Fig. 4 The electron density n_e (red), the electronic relaxation time τ (black), the effective electron mass m^* (orange, here m_0 is rest electron mass), and the electronic localization factor c (green) of BL MoS_2 as a function of magnetic field. The curves are drawn to guide the eye.

3.2 Key electronic parameters

In this study, we use Eq. (7) to fit four groups of experimental data (i.e., $\sigma_{1\pm}(\omega)$ and $\sigma_{2\pm}(\omega)$) and, thus, to obtain four electronic parameters (i.e., τ, ω_c or m^*, σ_0 or n_e, and c). In Fig. 4, we plot the electron density n_e (red), the electron relaxation time τ (black), the effective electron mass m^* (orange), and the electron localization factor c (green) for BL MoS_2 on a sapphire substrate as a function of the magnetic field at a fixed temperature of 80 K. We find that the electron density in BL MoS_2 decreases with increasing magnetic field, similar to the case of ML MoS_2 [37]. This is a typical feature of a 2D semiconductor [38]. This effect is mainly caused by electronic localization in the presence of strong magnetic field and of the charged impurity scattering [38]. Similar to the cases of ML MoS_2 [37] and bi- and tri-layer graphene [24], the electronic relaxation time in BL MoS_2 increases with B. This is mainly due to the fact that the radius of the cyclotron movement of an electron decreases with increasing B, which can reduce the strength or possibility of the effective electronic scattering from phonons and impurities [38]. It is shown in Fig. 4 that the effective electron mass increases slightly with B, which is another typical feature of a semiconductor based 2D electron gas [39] and is induced by magnetic confinement of electron motion [39].

We have shown that the effect of photon-induced electronic backscattering or localization can be present rather strongly in BL MoS_2 at $B = 0$ [18]. This effect can still be observed in the presence of magnetic field. However, we can see from Fig. 4 that the absolute value of the electronic localization factor decreases with increasing B, which is also in line with the trend of ML MoS_2 [37]. This indicates that the photon-induced electronic localization effect weakens as the magnetic field

increases. The physical reason behind this effect is that the electronic relaxation time τ (or the overall electronic scattering rate) increases (decreases) with increasing B (see Fig. 4) so that the possibility of electronic backscattering decreases with increasing B. Within the mechanism of the Drude–Smith model [36], under the action of optical driving an electron in a material experiences collisions which are randomly distributed in time but with an average time interval τ between collision events. Therefore, a longer relaxation time τ can lead to a smaller persistence of the change of initial velocity for an electron after a backscattering event, namely a smaller value of $|c|$ can be achieved by a longer τ in general. It should be noted that we normally cannot directly measure the electronic localization induced by backscattering using the conventional transport experiments. Using the Drude–Smith model to fit the experimental results obtained from, e.g., THz TDS, we can examine this effect optically and obtain quantitatively the localization factor c in electronic gas systems.

With the MO conductivities, we can evaluate the corresponding DC MO mobilities. From Eq. (5), the longitudinal DC mobility at $\omega \to 0$ is given by

$$\mu_{xx}(B) = \mu_0 \frac{(1+c) + (\omega_c\tau)^2(1-c)}{\left(1+(\omega_c\tau)^2\right)^2}, \tag{8}$$

with $\mu_0 = e\tau/m^*$ being the DC mobility at $B = 0$ and in the absence of electronic localization. Thus, the mobility measured optically at $B = 0$ is $\mu_{xx}(0) = \mu_0(1+c)$. Using $\tau \sim 94$ fs, $m^*/m_0 \sim 0.55$ and $c \sim -0.418$ obtained from our measurement at $B \to 0$ (see Fig. 4), we find $\mu_{xx}(0) \sim 174$ $\mathrm{cm^2 \cdot V^{-1} \cdot s^{-1}}$ at $T = 80$ K, which is a typical value of electron mobility in $2H$-stacking BL MoS_2. We note that $\mu_{xx}(0) \sim 107$ $\mathrm{cm^2 \cdot V^{-1} \cdot s^{-1}}$ at room-temperature was reported for $2H$-stacking BL MoS_2 [40]. The electron mobility at 80 K should be larger than that at 300 K due to the reduction of electron–phonon scattering.

The effective electron mass m^* is one of the most important electronic parameters in an electronic material, which affects most of the electronic, transport and optical properties of the material and device. It can normally be measured via cyclotron resonance (CR) effect [38, 41] where an optical absorption peak is observed when $\omega \sim \omega_c = eB/m^*$. From Fig. 3, we do not see the CR effect in both $\sigma_{1\pm}(\omega)$ and $\sigma_{2\pm}(\omega)$. This is because the $2H$-stacking BL MoS_2 is with a relatively heavy m^* around the Q-point. The measurable CR effect needs the application of B field larger than 8 T and/or the measurement in a wider frequency regime larger than 1.0 THz. Moreover, another necessary condition to observe the CR effect is $\omega\tau \sim \omega_c\tau > 1$. Because τ in our BL MoS_2 sample is less than 0.14 ps (see Fig. 4) even at $B = 8$ T and $T = 80$ K, this condition is not satisfied in radiation frequency regime from 0.1 to 1.0 THz. In this study, we use MO THz TDS to measure m^* around the Q-point in $2H$-stacking BL MoS_2 via fitting the experimental results with theoretical formulas. The value of $m^*/m_0 \sim 0.566$ obtained here is very close to that obtained from DFT calculation [18, 42]. Together with our measurements of m^* in bi- and tri-layer graphene [24], we find that MO THz TDS is a powerful technique for determination of m^* in electronic materials with heavy m^* and low electron mobility under the non-resonance condition.

4 Conclusions

In this study, we have investigated the THz MO properties of $2H$-stacking BL MoS_2 on sapphire substrate by using THz TDS in combination with the polarization test in the presence of magnetic field in the Faraday geometry. The measurements have been conducted at a fixed temperature of 80 K and magnetic fields ranging from 0 to 8 T. The real and imaginary parts of the MO conductivities for the BL MoS_2 sample have been obtained. We have applied the generalized MO Drude–Smith formula for MO conductivities, developed by us previously, to fit these experimental results. Through fitting, we have determined magneto-optically the key electronic parameters of the $2H$-stacking BL MoS_2 such as the electron density, the electronic relaxation time, the effective electron mass, and the photon-induced electronic localization factor in $2H$-stacking BL MoS_2. The magnetic field dependence of these parameters have been examined. In particular, the effective electron mass m^* around the Q-point in $2H$-stacking BL MoS_2 has been measured experimentally for the first time under the non-resonance condition. The m^* obtained here is very close to theoretical value calculated by the DFT approach. We believe that the findings from this research work can provide the valuable insights into the fundamental physical properties of BL MoS_2 and other BL TMD structures to be applied as advanced electronic and optoelectronic materials and devices.

Declarations The authors declare that they have no competing interests and there are no conflicts.

Electronic supplementary materials The online version contains supplementary material available at https://doi.org/10.1007/s11467-024-1425-4 and https://journal.hep.com.cn/fop/EN/10.1007/s11467-024-1425-4.

Acknowledgements This work was supported by the National Natural Science Foundation of China (NSFC) (Grant Nos. U2230122 and U2067207) and Shenzhen Science and Technology Program (No. KQTD20190929173954826).

References

1. D. Akinwande, C. Huyghebaert, C. H. Wang, M. I.

Serna, S. Goossens, L. J. Li, H. S. Wong, and F. H. L. Koppens, Graphene and two-dimensional materials for silicon technology, *Nature* 573(7775), 507 (2019)
2. D. Xiao, G. B. Liu, W. Feng, X. Xu, and W. Yao, Coupled spin and valley physics in monolayers of MoS_2 and other group-VI dichalcogenides, *Phys. Rev. Lett.* 108(19), 196802 (2012)
3. Y. Cao, V. Fatemi, S. Fang, K. Watanabe, T. Taniguchi, E. Kaxiras, and P. Jarillo-Herrero, Unconventional superconductivity in magic-angle graphene superlattices, *Nature* 556(7699), 43 (2018)
4. M. L. Lin, Q. H. Tan, J. B. Wu, X. S. Chen, J. H. Wang, Y. H. Pan, X. Zhang, X. Cong, J. Zhang, W. Ji, P. A. Hu, K. H. Liu, and P. H. Tan, Moiré phonons in twisted bilayer MoS_2, *ACS Nano* 12(8), 8770 (2018)
5. K. F. Mak, D. Xiao, and J. Shan, Light–valley interactions in 2D semiconductors, *Nat. Photonics* 12(8), 451 (2018)
6. M. Liao, Z. Wei, L. Du, Q. Wang, J. Tang, H. Yu, F. Wu, J. Zhao, X. Xu, B. Han, K. Liu, P. Gao, T. Polcar, Z. Sun, D. Shi, R. Yang, and G. Zhang, Precise control of the interlayer twist angle in large scale MoS_2 homostructures, *Nat. Commun.* 11(1), 2153 (2020)
7. T. Y. Zhang, J. T. Wang, P. Wu, A. Y. Lu, and J. Kong, Vapour-phase deposition of two-dimensional layered chalcogenides, *Nat. Rev. Mater.* 8(12), 799 (2023)
8. C. Fox, Y. L. Mao, X. Zhang, Y. Wang, and J. Xiao, Stacking order engineering of two-dimensional materials and device applications, *Chem. Rev.* 124(4), 1862 (2024)
9. K. F. Mak, D. Xiao, and J. Shan, Light–valley interactions in 2D semiconductors, *Nat. Photonics* 12(8), 451 (2018)
10. Q. Tong, H. Yu, Q. Zhu, Y. Wang, X. Xu, and W. Yao, Topological mosaics in moiré superlattices of van der Waals heterobilayers, *Nat. Phys.* 13(4), 356 (2017)
11. K. Seyler, P. Rivera, H. Yu, N. Wilson, E. Ray, D. Mandrus, J. Yan, W. Yao, and X. Xu, Signatures of moiré-trapped valley excitons in $MoSe_2/WSe_2$ heterobilayers, *Nature* 567(7746), 66 (2019)
12. G. Sharma, Tunable topological Nernst effect in two-dimensional transition-metal dichalcogenides, *Phys. Rev. B* 98(7), 075416 (2018)
13. M. Brotons-Gisbert, H. Baek, A. Molina-Sa'nchez, A. Campbell, E. Scerri, D. White, K. Watanabe, K. Taniguchi, C. Bonato, and B. D. Gerardot, Spin-layer locking of interlayer excitons trapped in moiré potentials, *Nat. Mater.* 19(6), 630 (2020)
14. Q. Tong, H. Yu, Q. Zhu, Y. Wang, X. Xu, and W. Yao, Topological mosaics in moiré superlattices of van der Waals heterobilayers, *Nat. Phys.* 13(4), 356 (2017)
15. K. F. Mak, C. Lee, J. Hone, J. Shan, and T. F. Heinz, Atomically thin MoS_2: A new direct-gap semiconductor, *Phys. Rev. Lett.* 105(13), 136805 (2010)
16. A. M. van der Zande, J. Kunstmann, A. Chernikov, D. A. Chenet, Y. M. You, X. X. Zhang, P. Y. Huang, T. C. Berkelbach, L. Wang, F. Zhang, M. S. Hybertsen, D. A. Muller, D. R. Reichman, T. F. Heinz, and J. C. Hone, Tailoring the electronic structure in bilayer molybdenum disulfide via interlayer twist, *Nano Lett.* 14(7), 3869 (2014)
17. A. Kormányos, V. Z'olyomi, V. I. Fal'ko, and G. Burkard, Tunable Berry curvature and valley and spin Hall effect in bilayer MoS_2, *Phys. Rev. B* 98(3), 035408 (2018)
18. X. Cheng, W. Xu, H. Wen, J. Zhang, H. Zhang, H. Li, F. M. Peeters, and Q. Chen, Electronic properties of 2*H*-stacking bilayer MoS_2 measured by terahertz time-domain spectroscopy, *Front. Phys.* 18(5), 53303 (2023)
19. M. Xia, B. Li, K. Yin, G. Capellini, G. Niu, Y. Gong, W. Zhou, P. M. Ajayan, and Y. H. Xie, Spectroscopic signatures of AA′ and AB stacking of chemical vapor deposited bilayer MoS_2, *ACS Nano* 9(12), 12246 (2015)
20. R. Ulbricht, E. Hendry, J. Shan, T. F. Heinz, and M. Bonn, Carrier dynamics in semiconductors studied with time-resolved terahertz spectroscopy, *Rev. Mod. Phys.* 83(2), 543 (2011)
21. J. Lloyd-Hughes and T. I. Jeon, A review of the terahertz conductivity of bulk and nano-materials, *Int. J. Infrared Millim. Terahertz Waves* 33(9), 871 (2012)
22. M. Schubert, P. Kühne, V. Darakchieva, and T. Hofmann, Optical Hall effect model description: Tutorial, *J. Opt. Soc. Am. A* 33(8), 1553 (2016)
23. A. J. Campbell, M. Brotons-Gisbert, H. Baek, V. Vitale, T. Taniguchi, K. Watanabe, J. Lischner, and B. D. Gerardot, Exciton–polarons in the presence of strongly correlated electronic states in a $MoSe_2/WSe_2$ moiré superlattice, *npj 2D Mater. Appl.* 6, 79 (2022)
24. H. Mei, W. Xu, C. Wang, H. Yuan, C. Zhang, L. Ding, J. Zhang, C. Deng, Y. Wang, and F. M. Peeters, Terahertz magneto-optical properties of bi- and tri-layer graphene, *J. Phys.: Condens. Matter* 30(17), 175701 (2018)
25. S. Schöche, J. S. Shi, A. Boosalis, P. Kühne, C. M. Herzinger, J. A. Woollam, W. J. Schaff, L. F. Eastman, M. Schubert, and T. Hofmann, Terahertz optical-Hall effect characterization of two-dimensional electron gas properties in AlGaN/GaN high electron mobility transistor structures, *Appl. Phys. Lett.* 98(9), 092103 (2011)
26. Y. Yu, C. Li, Y. Liu, L. Su, Y. Zhang, and L. Cao, Controlled scalable synthesis of uniform, high-quality monolayer and few-layer MoS_2 films, *Sci. Rep.* 3(1), 1866 (2013)
27. X. Wang, H. Feng, Y. Wu, and L. Jiao, Controlled synthesis of highly crystalline MoS_2 flakes by chemical vapor deposition, *J. Am. Chem. Soc.* 135(14), 5304 (2013)
28. S. Hussain, M. A. Shehzad, D. Vikraman, M. Z. Iqbal, J. Singh, M. F. Khan, J. Eom, Y. Seo, and J. Jung, Controlled synthesis and optical properties of polycrystalline molybdenum disulfide atomic layers grown by chemical vapor deposition, *J. Alloys Compd.* 653, 369 (2015)
29. A. M. van der Zande, J. Kunstmann, A. Chernikov, D. A. Chenet, Y. M. You, X. X. Zhang, P. Y. Huang, T. C. Berkelbach, L. Wang, F. Zhang, M. S. Hybertsen, D. A. Muller, D. R. Reichman, T. F. Heinz, and J. C. Hone, Tailoring the electronic structure in bilayer molybdenum disulfide via interlayer twist, *Nano Lett.* 14(7), 3869 (2014)
30. F. Ullah, J.-H. Lee, Z. Tahir, A. Samad, C. T. Le, J. Kim, D. Kim, M. U. Rashid, S. Lee, K. Kim, H. Cheong, J. I. Jang, M.-J. Seong, and Y. S. Kim, Selective growth and robust valley polarization of bilayer 3*R*-MoS_2, *Appl. Mater. & Inter.* 13(48), 57588 (2021)

31. M. Hangyo, T. Nagashima, and S. Nashima, Spectroscopy by pulsed terahertz radiation, *Meas. Sci. Technol.* 13(11), 1727 (2002)
32. L. F. Man, W. Xu, Y. M. Xiao, H. Wen, L. Ding, B. Van Duppen, and F. M. Peeters, Terahertz magneto-optical properties of graphene hydrodynamic electron liquid, *Phys. Rev. B* 104(12), 125420 (2021)
33. O. Morikawa, A. Quema, S. Nashima, H. Sumikura, T. Nagashima, and M. Hangyo, Faraday ellipticity and Faraday rotation of a doped-silicon wafer studied by terahertz time-domain spectroscopy, *J. Appl. Phys.* 100(3), 033105 (2006)
34. M. Tinkham, Energy gap interpretation of experiments on infrared transmission through superconducting films, *Phys. Rev.* 104(3), 845 (1956)
35. F. W. Han, W. Xu, L. L. Li, and C. Zhang, A generalization of the Drude–Smith formula for magneto-optical conductivities in Faraday geometry, *J. Appl. Phys.* 119(24), 245706 (2016)
36. N. V. Smith, Classical generalization of the Drude formula for the optical conductivity, *Phys. Rev. B* 13, 4212 (2013)
37. H. Wen, W. Xu, C. Wang, D. Song, H. Y. Mei, J. Zhang, and L. Ding, Magneto-optical properties of monolayer MoS_2–SiO_2/Si structure measured via terahertz time-domain spectroscopy, *Nano Select* 1, 90 (2020)
38. W. G. Spitzer and H. Y. Fan, Determination of optical constants and carrier effective mass of semiconductors, *Phys. Rev.* 106(5), 882 (1957)
39. F. M. Peeters, X. G. Wu, and J. T. Devreese, Cyclotron mass of a polaron in two dimensions, *Phys. Rev. B* 34(2), 1160 (1986)
40. L. Liu, T. Li, L. Ma, W. Li, S. Gao, W. Sun, R. Dong, X. Zou, D. Fan, L. Shao, C. Gu, N. Dai, Z. Yu, X. Chen, X. Tu, Y. Nie, P. Wang, J. Wang, Y. Shi, and X. Wang, Uniform nucleation and epitaxy of bilayer molybdenum disulfide on sapphire, *Nature* 605(7908), 69 (2022)
41. J. W. Hodby, G. P. Russell, F. M. Peeters, J. T. Devreese, and D. M. Larsen, Cyclotron resonance of polarons in the silver halides: AgBr and AgCl, *Phys. Rev. Lett.* 58(14), 1471 (1987)
42. A. Mukhopadhyay, S. Kanungo, and H. Rahaman, The effect of the stacking arrangement on the device behavior of bilayer MoS_2 FETs, *J. Comput. Electron.* 20(1), 161 (2021)